Materials Chemistry and Physics 315 (2024) 129022

Contents lists available at ScienceDirect

Materials Chemistry and Physics

journal homepage: www.elsevier.com/locate/matchemphys

Nano-Ni/Cu decorated iron oxide for catalytic reduction of 4-nitrophenol

Anname Lourens [a], Anzel Falch [b,*], Rehana Malgas-Enus [a]

[a] Stellenbosch University, Department of Chemistry and Polymer Science, Private Bag X1, Matieland, 7602, Stellenbosch, South Africa
[b] Molecular Sciences Institute, School of Chemistry, University of the Witwatersrand, Johannesburg, South Africa

HIGHLIGHTS

- Fast, cost-effective, and simple impregnation method for SPION@Ni/Cu catalysts.
- SPION@Ni/Cu (0.2:1 M^{2+}:SPIONs mass ratio) exhibited a competitive k_{app} of 0.103 s^{-1}.
- Easy separation via magnetic decantation and recyclable for up to 10 times.

GRAPHICAL ABSTRACT

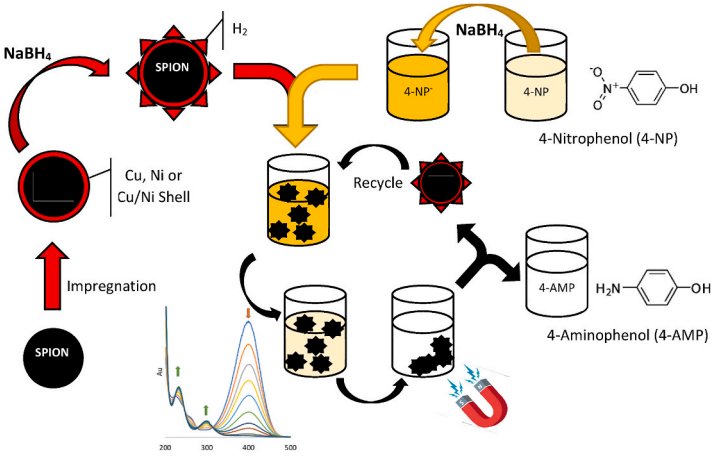

ARTICLE INFO

Keywords:
Catalyst immobilization
4-Nitrophenol removal
Magnetic nanoparticle catalysts
Supported catalysts
Wastewater treatment

ABSTRACT

This study utilized fast, affordable, and simple impregnation methods to produce a more affordable, highly active, and recyclable Cu and Ni magnetic nanocatalyst for the removal of 4-nitrophenol (4-NP) from wastewater. The core-shell synthesis methods used capture the magnetic capability at the center via a superparamagnetic iron oxide nanoparticle (SPION) core while utilizing the catalytically active Cu and Ni atoms on its surface. Monometallic coated Ni and Cu SPIONs (SPION@Ni) and SPION@Cu) as well as bimetallic Cu/Ni coated SPIONs (SPION@Ni/Cu) ranging between 15 and 21 nm were evaluated for the reduction of 4-NP to 4-aminophenol (4-AMP) in the presence of excess $NaBH_4$ as reducing agent. The Ultraviolet–visible (UV–Vis) spectroscopy method was utilized to monitor the catalytic kinetic reaction. The assessed nanoparticles demonstrated enhanced activity in the progression from SPION@Ni to SPION@Cu, with SPION@Ni/Cu nanoparticles proving to be the most efficient, particularly with AL18 (SPION@Ni/Cu (1(SPION):0.2(M^{2+})) achieving a k_{app} of 0.103 s^{-1}. In addition, **AL18** was easily separated via magnetic decantation and successfully reused for up to ten consecutive reactions.

* Corresponding author.
E-mail address: anzel.falch@wits.ac.za (A. Falch).

https://doi.org/10.1016/j.matchemphys.2024.129022
Received 14 August 2023; Received in revised form 23 January 2024; Accepted 1 February 2024
Available online 1 February 2024

1. Introduction

The growing population has resulted in a drastic increase in industrial and agricultural activities. The lack of efficient control over waste disposal of these industries has resulted in various pollutants escaping into our natural water sources [1]. As these pollutants are often toxic and harmful to living organisms, research efforts have focused on the efficient removal by absorption or degradation [2]. One such example includes the catalytic reduction of 4-NP that has commonly been used as a "model catalytic reaction" [3]. These aromatic nitro compounds are commonly used in synthesis of pharmaceuticals, dyes, explosives, pesticides and herbicides as well as paper and leather manufacturing and are known to be toxic and carcinogenic due to the presence of a nitro group [4,5]. Although the removal of these toxins has been extensively studied, there is still a need for more affordable, highly recyclable, stable catalysts to further streamline the process and decrease chemical waste [8,12–19,21].

Magnetic nanoparticles (MNPs) have gained a lot of attention as heterogenous catalysts for catalytic degradation of water pollutants due to their magnetic character, making them easy to remove and recycle [1,2,6]. The small nanostructure allows for high surface-to-volume ratio and easy manipulation of the surface to optimize the catalytic activity [7,8].

Core-shell magnetic NPs can be tailored to benefit from the magnetic core while utilizing highly active metals on the surface [11]. Metals such Pt, Rh, Pd and Ag/Ni have been utilized in the shell structure of MNPs and resulted in relatively good yields for nitroarene reduction [9,10,12–19]. These metals are however scarce and very expensive and utilize complicated methods such as coating or grafting to sufficiently immobilize the metal NP onto the SPION surface [30].

Recent studies done by Matinise et al. showed excellent reduction capability of Cu_{55} NPs [8]. These NPs were however unstable and easily agglomerated causing a decrease in activity. This was overcome by replacing some of the Cu atoms with Au atoms to generate a bimetallic structure. Research has shown that the immobilization of Cu on SPIONs allow for stabilized and recyclable nano-catalysts, hence this study thus focusses on the use of more affordable metals immobilized on the SPION surface via easy and fast impregnation methods [20]. These metals include highly active Cu [8] and less active but more affordable Ni NPs [21]. Previous studies done also proved that introducing additional NPs onto the SPION surface also greatly stabilize the active NPs as well as the SPION core by reducing oxidation and agglomeration of the said NPs [20].

These NPs were immobilized as both monometallic shells (SPION@Ni and SPION@Cu) as well as bimetallic shells (SPION@Ni/Cu) and their catalytic activities compared. The study shows how simple and affordable NPs can be utilized as efficient and recyclable magnetic catalyst to improve water quality in a more cost-efficient manner.

2. Experimental section

2.1. Materials and instrumentation

$FeSO_4{\cdot}7H_2O$, $FeCl_3{\cdot}6H_2O$, $NiCl_2{\cdot}6H_2O$, $Ni(NO_3)_2{\cdot}6H_2O$, $CuCl_2{\cdot}2H_2O$, $Cu(NO_3)_2{\cdot}2.5H_2O$, $NaBH_4$, 33 % NH_4OH (aqueous solution), $NH_2NH_2{\cdot}H_2O$ and EtOH were purchased from Sigma-Aldrich and used without further purification. The water used in all the processes was prepared in a Milli-Q water purification system. FT-IR (KBr) spectrum was measured in the range 4000–400 cm^{-1} using analytical grade KBr salt (Sigma-Aldrich). ICP-OES was recorded on a Spectro Arcos FHS 12 spectrometer which was first calibrated with Fe, Ni and Cu standards (Merck) in the range 0–100 ppm. UV–Vis characterization was performed on Shimadzu Spectrophotometer UV-1800 by sonicating the NP in ethanol and transferring it to a 1 cm path length quartz cuvette wherein absorbance was measured in the range 190–900 nm. The toxin removal processes were also monitored on this Shimadzu Spectrophotometer UV-1800 and described in section 2.5 and 2.6. Scanning electron microscopy (SEM) images of the NPs were produced on an FEI Quanta FEG 250 microscope with integrated energy-dispersive X-ray spectroscopy (EDS) to map the Ni, Cu and Fe atoms. Lastly, HR-TEM imaging was performed on a Tecnai G2 F20 microscope (Thermo Fisher).

2.2. Synthesis of *SPIONs*

SPIONs were synthesized, as described in our previous work [20], by combining $FeSO_4{\cdot}7H_2O$ and $FeCl_3{\cdot}6H_2O$ in a 1:2 mol ratio in degassed water at 60 °C. The Fe(II) and Fe(III) ions were co-precipitated under basic conditions upon dropwise addition of 33 % NH_4OH aqueous solution 1:10 Fe:NH_4OH mole ratio and resulted in a black precipitate formation. This reaction was stirred for 30 min whereafter the solid was isolated by magnetic decantation followed by repetitive washing with distilled H_2O until the solution was neutralized. The black solid was then washed with ethanol and dried at 60 °C for 24 h.

2.3. Immobilization of Ni and Cu NPs

Simple impregnation methods, as discussed in our previous paper [20] and illustrated (Fig. 1 and Table 1), were utilized in this study to reduce $NiCl_2$ (**AL01-AL03**), $Ni(NO_3)_2$ (**AL04- AL06**), $CuCl_2$ (**AL07-AL09**), $Cu(NO_3)_2$ (**AL10- AL12**) as well as a combination of $NiCl_2/CuCl_2$ (**AL13-AL15**) and $Ni(NO_3)_2/Cu(NO_3)_2$ (**AL16-AL18**) onto the SPION surface. Lourens et al. described this immobilization method to occur in 3 steps. First, coordination of the M^{2+} ions to the hydroxyl surface, second the reduction of M^{2+} to M^0 and lastly the evolutionary repetition of step 1 and 2 [20].

In this article both $NaBH_4$ (**AL02, AL03, AL05, AL06, AL08, AL09, AL11, AL12, AL14, AL15, AL17** and **AL18**) and $NH_2NH_2{\cdot}H_2O$ (**AL01, AL03 AL05, AL07, AL10, AL13, AL16**) were utilized in their respective methodologies (please refer to ESI for details) to precipitate the active metals onto SPIONs. Additionally, two different mass ratios of metal salt-to-SPIONs, namely 1:1 and 0,2:1, were synthesized to compare their effect on the NP size and catalytic properties (Table 1). Magnetic decantation is used in the purification step of this method as it removes all the non-magnetic impurities that did not successfully attach to the SPION surface.

2.4. Catalytic reduction of 4-nitrophenol

SPION@Cu, SPION@Ni and SPION@Ni/Cu catalysts were evaluated

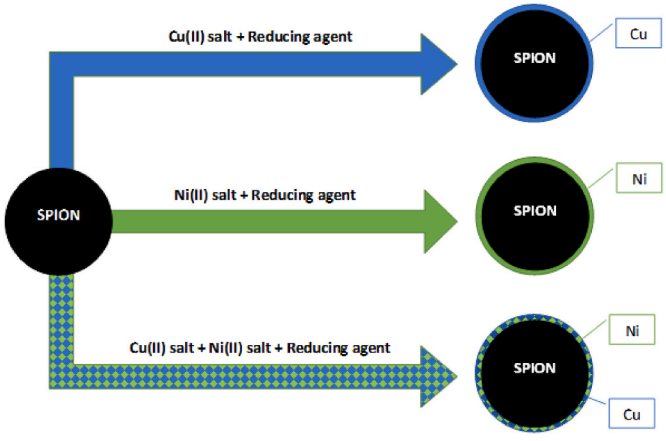

Fig. 1. Immobilization of Ni and Cu NPs onto the SPION surface through simple impregnation methods to synthesize Cu (blue), Ni (green) and Cu/Ni (green + blue) coated SPIONs. (For interpretation of the references to color in this figure legend, the reader is referred to the Web version of this article.)

Table 1
Name and description of magnetic nano-catalysts.

Sample code	Metal precursor used (M^{2+})	M^{2+}:SPIONs mass ratio	Reducing agent used
SPIONs			
AL01	$NiCl_2{\cdot}6H_2O$	1:1	$NH_2NH_2{\cdot}H_2O$
AL02	$NiCl_2{\cdot}6H_2O$	1:1	$NaBH_4$
AL03	$NiCl_2{\cdot}6H_2O$	0,2:1	$NaBH_4$
AL04	$Ni(NO_3)_2{\cdot}6H_2O$	1:1	$NH_2NH_2{\cdot}H_2O$
AL05	$Ni(NO_3)_2{\cdot}6H_2O$	1:1	$NaBH_4$
AL06	$Ni(NO_3)_2{\cdot}6H_2O$	0,2:1	$NaBH_4$
AL07	$CuCl_2{\cdot}2H_2O$	1:1	$NH_2NH_2{\cdot}H_2O$
AL08	$CuCl_2{\cdot}2H_2O$	1:1	$NaBH_4$
AL09	$CuCl_2{\cdot}2H_2O$	0,2:1	$NaBH_4$
AL10	$Cu(NO_3)_2{\cdot}2.5H_2O$	1:1	$NH_2NH_2{\cdot}H_2O$
AL11	$Cu(NO_3)_2{\cdot}2.5H_2O$	1:1	$NaBH_4$
AL12	$Cu(NO_3)_2{\cdot}2.5H_2O$	0,2:1	$NaBH_4$
AL13	$NiCl_2{\cdot}6H_2O + CuCl_2{\cdot}2H_2O$	1:1	$NH_2NH_2{\cdot}H_2O$
AL14	$NiCl_2{\cdot}6H_2O + CuCl_2{\cdot}2H_2O$	1:1	$NaBH_4$
AL15	$NiCl_2{\cdot}6H_2O + CuCl_2{\cdot}2H_2O$	0,2:1	$NaBH_4$
AL16	$Ni(NO_3)_2{\cdot}6H_2O + Cu(NO_3)_2{\cdot}2.5H_2O$	1:1	$NH_2NH_2{\cdot}H_2O$
AL17	$Ni(NO_3)_2{\cdot}6H_2O + Cu(NO_3)_2{\cdot}2.5H_2O$	1:1	$NaBH_4$
AL18	$Ni(NO_3)_2{\cdot}6H_2O + Cu(NO_3)_2{\cdot}2.5H_2O$	0,2:1	$NaBH_4$

for the reduction of 4-NP in the presence of excess $NaBH_4$. In a standard cuvette with total volume 4 mL, 100 μL of 4-NP (5 mM) was added to 1 mL of $NaBH_4$ (0.1 M) resulting in a bright yellow solution. Finally, 10 μL of catalyst (5.97 mM) was introduced and the solution subjected to UV–Vis measurements. The absorbance was measured every minute in the scanning range of 200–600 nm to monitor the conversion of 4-NP through the decrease in the 4-NP peak at 400 nm and a simultaneous increase in the 4-AMP peak at 300 nm. The apparent rate constant (k_{app}) was determined for each reaction from the linear slope using equation (1):

$$\ln\left(\frac{A}{A_{t=0}}\right) = \ln\left(\frac{C}{C_{t=0}}\right) = -k_{app}.t \qquad \text{Equation 1}$$

where A is the absorbance (at 400 nm) and C is the concentration of the 4-NP ion at each point in time while $A_{t=0}$ is the initial absorbance (at 400 nm) and $C_{t=0}$ is the initial concentration before introducing the catalyst. All the experiments were performed in triplicate and the averages reported.

2.5. Recycling studies

The reusability of **AL18** was evaluated in a standard cuvette containing 100 μL of 4-NP (5 mM), 1 mL of $NaBH_4$ (0.05 M), 100 μL of catalyst (5.97 mM) topped to 4 mL with distilled water. The reaction was prepared and monitored as described in section 2.4. After completion, the MNPs was isolated via magnetic decantation and washed repeatedly with deionized water. The catalyst was then introduced into a fresh reaction solution and again subjected to UV–Vis. This was repeated for 10 consecutive experiments.

2.6. Absorption of 4-nitrophenol

SPIONs, SPION@Cu, SPION@Ni and SPION@Ni/Cu catalysts were evaluated for the absorption of 4-NP in the absence of $NaBH_4$ 10 mg of NPs was added to 10 mL of 4-NP (5 mM) and the mixture shaken on 250 rpm for 24 h. The MNPs were then isolated via magnetic decantation and the solution subjected to UV–Vis measurements. The absorbance was measured in the scanning range 200–600 nm to monitor the decrease in the 4-NP peak at 320 nm.

3. Results and discussion

3.1. Synthesis and characterization of NPs

Utilizing SPIONs as a heterogeneous anchor not only allows for easy separation but also stabilize these previously unstable NPs [20]. During the SPIONs synthesis method, the solution turned from yellow to brown to black upon reduction while it simultaneously gained magnetic characteristics. These SPIONs are hydrophilic in nature due to the hydroxyl groups coordinated to the Fe surface [11]. Many studies have focused on the use of metal NPs immobilized on SPIONs for the reduction of 4-NP in the presence of $NaBH_4$. These catalysts are however not as feasible as their synthesis methods are complicated, expensive, and utilize expensive and rare metals such as Pt, Rh and Pd [12–19]. Ni and Cu is thus of great interest as it is affordable, abundantly available and has proven to be efficient in the reduction of 4-NP [8,21]. Easy, inexpensive, and fast immobilization of these active NPs on the SPION surface is of great interest as it can significantly reduce the production cost.

UV–Vis and FT-IR characterization of the NPs (Table 1) have been reported in our previous work (AL01-AL12) [20]. with the UV–Vis and FT-IR spectra of AL13-AL18 available in ESI Figure S1 and Fig. S2 respectively. UV–Vis proved successful reduction of Cu(II) and Ni(II) through the absence of their d-d transition bands at 258 nm and 390 nm respectively with similar peaks to that of SPOIN being pronounced [20]. FT-IR showed characteristic peaks for both the metal precursor salt anions as well as remains of the respective reducing agents attached to the NP surface. Briefly, for the spectra shown Fig. S1 (supporting information), the naked iron oxide NP SPIONs exhibit the characteristic Fe–O peak at ~574 cm^{-1}. When coating this iron oxide surface with Ni/Cu NPs, this peak shifts to a higher wavenumber ~580-589 cm^{-1} indicating that complexation has occurred. Ni–O stretching frequencies were observed for AL13-18 at 420 cm^{-1} proving that the Ni is present on the surface and bound to the oxygen atoms. The peaks observed for the anions introduced by the various metal salt precursors are observed at ~1050 cm^{-1} and ~1400 cm^{-1} for chlorides present on AL13-Al15 while N–O peaks were observed at 1450 cm^{-1} and 1630-1635 cm^{-1} for AL16-AL18.

As the magnetic decantation washing gets rid of any ions that are not anchored to the SPION surface, ICP-OES was recorded again to ensure that the Ni and Cu atoms are present on the nano-catalyst surface. The NPs were digested in aqua regia, at 80 °C for 6 h whereafter the dried residue was dissolved in 0.1 M nitric acid solution and the samples subjected to ICP-OES analysis. The metal content of three samples of each catalyst were determined per 1 mg sample and the average and standard deviation reported (ESI Table S1). As expected, higher Ni and Cu content was achieved for **AL02, AL05, AL08, AL11**, **AL14** and **AL17** when compared to **AL03, AL06, AL09, AL12, AL15** and **AL18** as the metal salt-to-SPION ratio was increased. This indicates that the evolution step continues until all of metal ions are reduced onto the SPION surface. When comparing the different reducing agents to one another it is seen that higher Ni and Cu content was observed for the $NaBH_4$ method (**AL02, AL05, AL11**) compared to the $NH_2NH_2{\cdot}H_2O$ method (**AL01, AL04, AL10**) due to the organic matter making up the mass in the $NH_2NH_2{\cdot}H_2O$ samples. This indicated that these organic molecules were possibly attached to the NP surface thus decreasing the metal content per 1 mg per sample.

In addition to the characterization techniques conducted in our previous work [20], SEM-EDS was used to analyze the surface of the Cu/Ni bimetallic NPs and ensure that homogeneous distribution of the Ni and Cu atoms on the SPION surface was achieved. The results in Fig. 2 show an even distribution of Fe (green), Cu (red) and Ni (white) atoms on both **AL14** and **AL17,** respectively. This indicates that the bimetallic coated SPIONs achieve homogeneous distribution of both metals irrespective of metal salt precursor used. This confirms that both the Cu and the Ni atoms are present on the surface of the magnetic NP rather than one or the other.

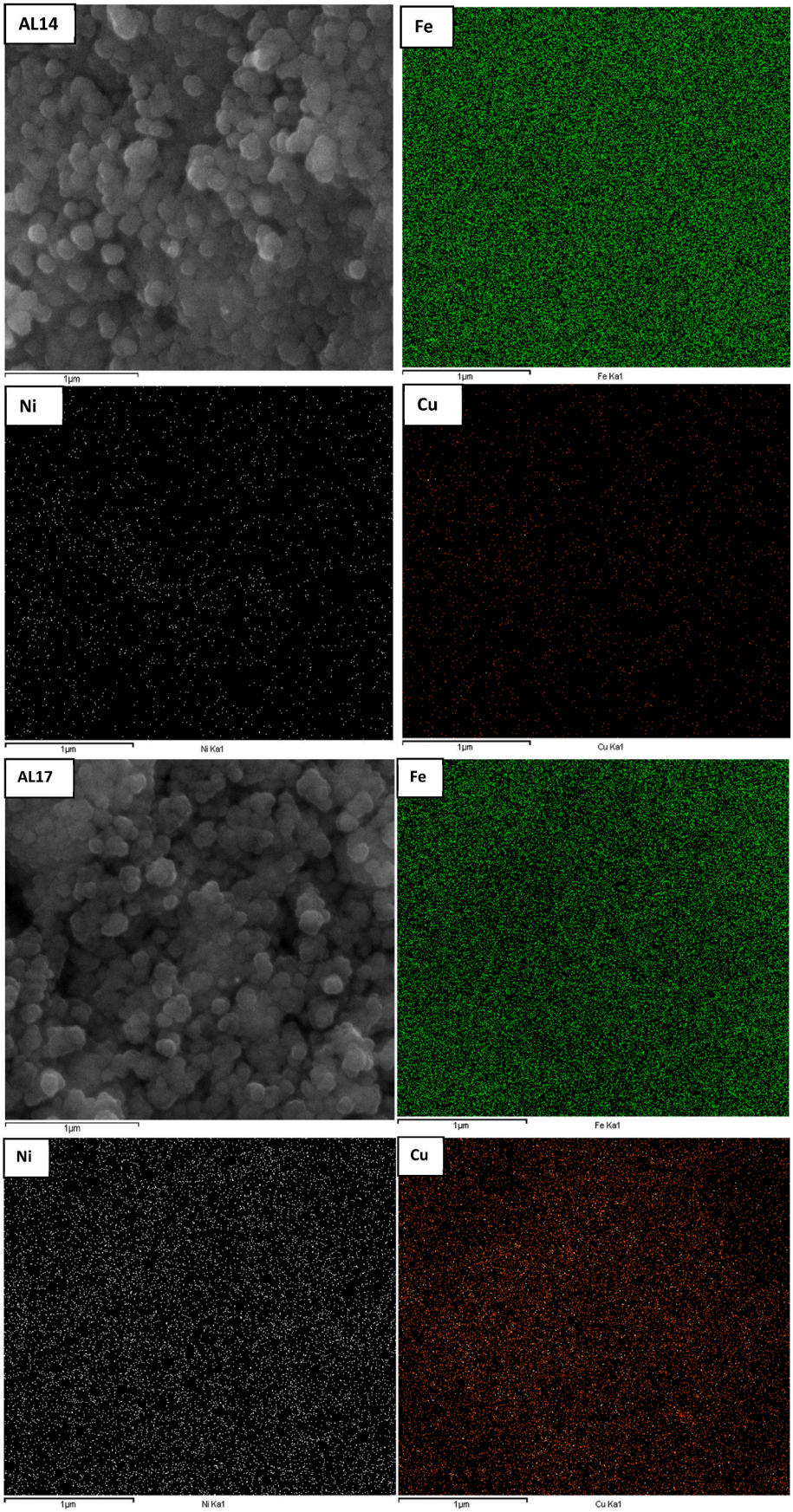

Fig. 2. SEM imaging along with EDS mapping of the Fe (green), Ni (white) and Cu (red) ions of bimetallic coated NPs, AL14 (top) and AL17 (bottom). (For interpretation of the references to color in this figure legend, the reader is referred to the Web version of this article.)

HR-TEM shown in Fig. 3 show monodispersed, amorphous NPs of a similar average size range of 15–21 nm in diameter. The TEM images show no sign of agglomeration of the coated NPs indicating that the anchoring of the Ni and Cu on the relatively stable magnetite supports allow for stabilization of the unstable metal NPs while simultaneously working as a size determining template [20]. This template allows for similar size and structure throughout. Very little difference was seen for the NPs using different reducing agents.

3.2. Reproducibility studies

The reproducibility for synthesis of these NPs were studied. This was achieved by repeating the synthesis and characterization methods discussed in section 2.2. - 2.3. and comparing the HR-TEM results in Table 2. The results showed similar particle sizes, within a 5 nm size difference, obtained for the first batch of catalyst prepared in the year 2021 vs the second batch of catalysts prepared in the year 2022. The results indicated that the SPIONs prepared as a precursor drastically influences the overall NP size achieved after coating as a larger SPION particle was used in 2022, resulting in overall larger NPs throughout. This is expected as the SPIONs function as a template onto which the Cu and Ni NPs grow to achieve larger NPs. Both these batches showed no sign of agglomeration indicating that the methods used resulted in relatively stable NPs.

Table 2
HR-TEM analysis determining particle sizes for Cu, Ni and Cu/Ni NPs synthesized in duplicate.

Sample code	Average size 2021 (nm)	Average size 2022 (nm)	Difference (nm)
SPIONs	12.0 ± 1.5	13.1 ± 1.1	+1.1
AL01	16.5 ± 2.5	15.6 ± 1.7	−0.9
AL02	15.4 ± 2.3	15.4 ± 2.8	–
AL03	15.7 ± 1.9	18.5 ± 2.9	+2.8
AL04	13.6 ± 2.0	16.0 ± 2.4	+2.4
AL05	15.2 ± 2.3	16.9 ± 2.7	+1.7
AL06	13.5 ± 1.5	16.5 ± 2.3	+3.0
AL07	15.3 ± 2.2	18.0 ± 2.2	+2.7
AL08	13.6 ± 2.4	18.3 ± 2.8	+3.0
AL09	15.4 ± 2.4	16.6 ± 2.3	+1.2
AL10	13.7 ± 1.7	16.9 ± 2.7	+3.2
AL11	12.9 ± 2.0	17.6 ± 2.7	+4.7
AL12	13.9 ± 2.0	16.4 ± 2.2	+2.5
AL13	14.0 ± 1.8	16.2 ± 2.3	+2.2
AL14	13.3 ± 1.7	15.1 ± 2.9	+1.8
AL15	15.2 ± 1.2	18.3 ± 2.4	+3.1
AL16	15.2 ± 1.9	18.3 ± 2.4	+3.1
AL17	14.1 ± 2.2	15.9 ± 1.9	+1.8
AL18	14.8 ± 2.5	17.4 ± 2.6	+2.6

3.3. 4-Nitrophenol removal

4-NP is a pollutant that can take up different forms depending on its environment [22]. The various forms determine the affinity of the

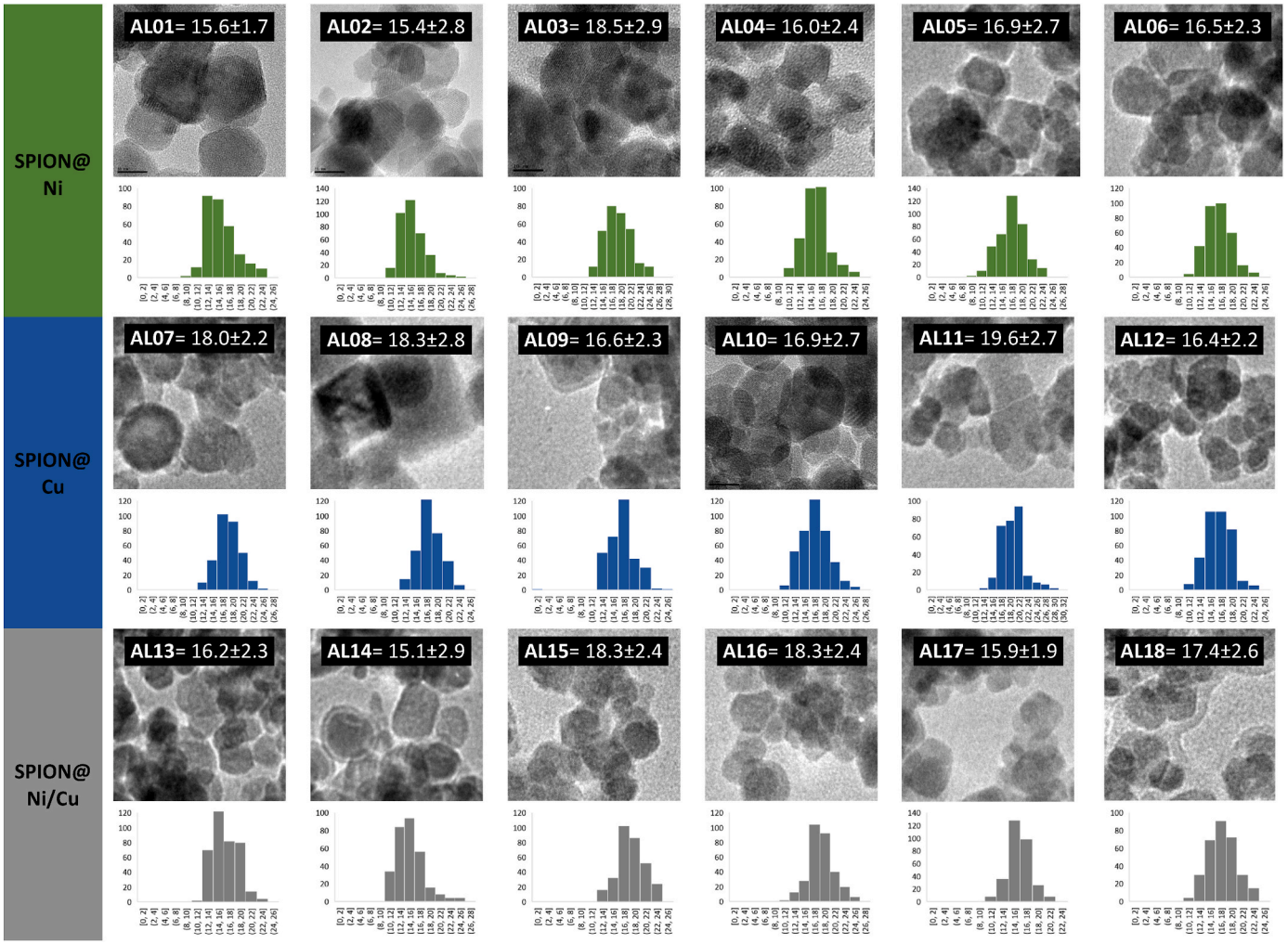

Fig. 3. HR-TEM micrographs on a 10 nm scale size and size distribution curves. The size distribution histograms have a bin width of 2.0.

reactant to the catalyst and thus determine whether the reaction will be taking place. These compounds all give distinctive peaks in the UV–Vis region as seen in Fig. 4 allowing for an easy way of monitoring the reaction through UV–Vis Spectrophotometry. The 4-NP is clear and absorbs light at 320 nm and 220 nm. The 4-Nitrophenolate ion (4-NP$^-$) is bright yellow in color and absorbs at 400 nm and 230 nm whereas the 4-AMP is clear and absorbs at 300 nm and 235 nm.

3.3.1. 4-Nitrophenol absorption

During the first set of blank reactions, the absorption of the 4-NP was monitored by introducing the SPIONs, **AL01**, **AL07** and **AL13** model catalysts, to a solution containing 4-NP without $NaBH_4$. These reactions were mixed for 24 h and analyzed with UV–Vis where it showed no decrease in the 4-NP peak at 320 nm. This indicated that the 4-NP molecule needs to be transformed to the 4-NP$^-$ anion before it can absorb onto the NP surface for absorption to occur. It also shows that although the NP contains hydrazine on the surface it was not able to reduce the pollutant without $NaBH_4$ as a H_2 supply.

3.3.2. 4-Nitrophenol reduction

The conversion of 4-NP to 4-AMP was chosen as a model reaction to monitor the catalytic capability of Ni, Cu and Ni/Cu NPs immobilized on the SPION surface. This reaction was monitored by UV–Vis over time by monitoring the gradual decrease in the 4-NP$^-$ peak at 400 nm and the subsequent increase in the 4-AMP peak at 300 nm seen in Fig. 5. Firstly, a blank containing 4-NP, $NaBH_4$ in aqueous solution was evaluated and showed no change in these critical peaks indicating that a catalyst is required to facilitate the reaction and that the reaction will take place solely on the NP surface [8]. Secondly, the naked **SPIONs** were evaluated in the presence of $NaBH_4$ and showed no conversion after 24 h. This indicates that the Fe ions are inactive in reducing this pollutant and more active surface ions such as Ni and Cu are required. The SPION core thus solely acts as an immobilizer for the active metals which is capable of stabilizing the active NP structure as a shell. **AL13** was then evaluated in the presence of $NaBH_4$ yielding the conversion UV–Vis spectra seen in Fig. 5. The isosbestic points present at 223 nm, 245 nm, 279 nm and 315 nm indicates that 4-NP$^-$ is completely reduced to 4-AMP and that no side reactions occurred during this time study [23].

The kinetics involved with 4-NP reduction has been studied extensively and it has been shown that this reaction follows the Langmuir Hinshelwood (LH) kinetic model [8,24,25]. This model states that both the 4-NP and the H_2 should coordinate to the NP surface before the reaction can take place.

3.3.2.1. 4-Nitrophenol reduction optimization. The bimetallic coated **AL13** was further used as a model catalyst in the optimization of this reaction. This catalyst consists of a SPION core coated with $CuCl_2$ and

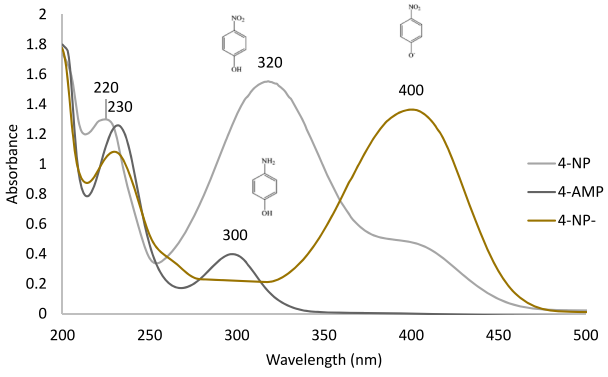

Fig. 4. UV–Vis absorption of 4-NP at 320 nm and 220 nm, 4-NP$^-$ at 400 nm and 4-AMP at 300 nm and 235 nm.

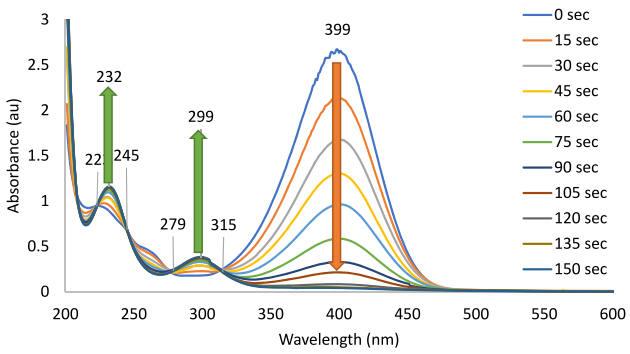

Fig. 5. Time dependent UV–Vis Spectra of 4-NP$^-$ (↓ 400 nm) reduction to 4-AMP (↑ 300 nm and ↑ 230 nm) with isosbestic points at 223 nm, 245 nm, 279 nm and 315 nm.

$NiCl_2$ in the presence of hydrazine as a reducing agent. This reaction started immediately after addition of the catalyst, without an induction time being present, indicating that no surface restructuring was necessary to coordinate the reactants under these conditions [26]. The catalyst was evaluated in a range of 4-NP, $NaBH_4$ and catalyst concentrations to determine the optimum reaction conditions.

During the first set of optimization reactions, the $NaBH_4$ and catalyst concentrations were kept constant while varying the 4-NP concentrations (1.25–5 mM) (Fig. 6a). A drop in the k_{app} value was observed with an increase in the 4- NP concentration. This is due to the strong absorption of 4-NP compared to $NaBH_4$ [27]. This results in the NP being crowded in 4-NP with very little open sites for H_2 to coordinate. Both these reagents need to be supported on the NP surface for the reaction to occur, and a low concentration of H_2 on the NP surface results in the reaction to occur much slower. The 4-NP concentration was then kept constant at 5 mM for the remaining catalytic runs as this was the maximum detection limit of the UV spectrometer used.

Excess $NaBH_4$ was added to 4-NP as prescribed by Ref. [8]. The effect of increased $NaBH_4$ was evaluated and showed to be directly related to the k_{app} value (Fig. 6b). This indicated that most active sites are occupied by hydrogen species and the increase in H^- concentration resulted in an increased rate of coordination, thus increasing the reaction rate [8,25]. This increase is linearly related to the $NaBH_4$ concentration. Therefore, 100 mM was chosen as the optimum concentration to compare the catalysts in their reductive capability as the rate is slow enough to see a significant difference in catalyst activity.

The catalyst concentration was also varied from 1.5 to 9 mmol/L while keeping the 4-NP and $NaBH_4$ concentrations constant and showed a linear increase as the catalyst concentration increased (Fig. 6c). This is expected and a well reported phenomenon as more active sites are available for the reaction to take place [8,14].

Lastly, the effect of temperature was studied by testing **AL13** at 283 K, 293 K, 313 K and 323 K respectively under constant catalyst loading of 5.97 mM, 100 mM $NaBH_4$ and 5 mM 4-NP (Fig. 6d). The temperature showed to be linearly proportional to the k_{app} achieved as described by collision theory. This theory explains that the vigorous movement of 4-NP molecules are enhanced when increasing the heat energy supplied to the reaction, thus increasing the chance for collisions to occur resulting in an increased reaction rate [8,14].

These rate constants achieved at different temperatures were then used to calculate various thermodynamic parameters (Table 3) such as the apparent activation energy (Ea_{app}), enthalpy ($\Delta H‡$), entropy ($\Delta S‡$), Gibbs energy ($\Delta G‡$) and pre-exponential factor (A) using the appropriate equations below, where R is the ideal gas constant (8.314 J/K. Mol), h is Planck's constant (6.63×10^{-34} J s), k_B is the Boltzmann constant (1.38×10^{-23} J/K and T is the absolute temperature (K).

Arrhenius equation:

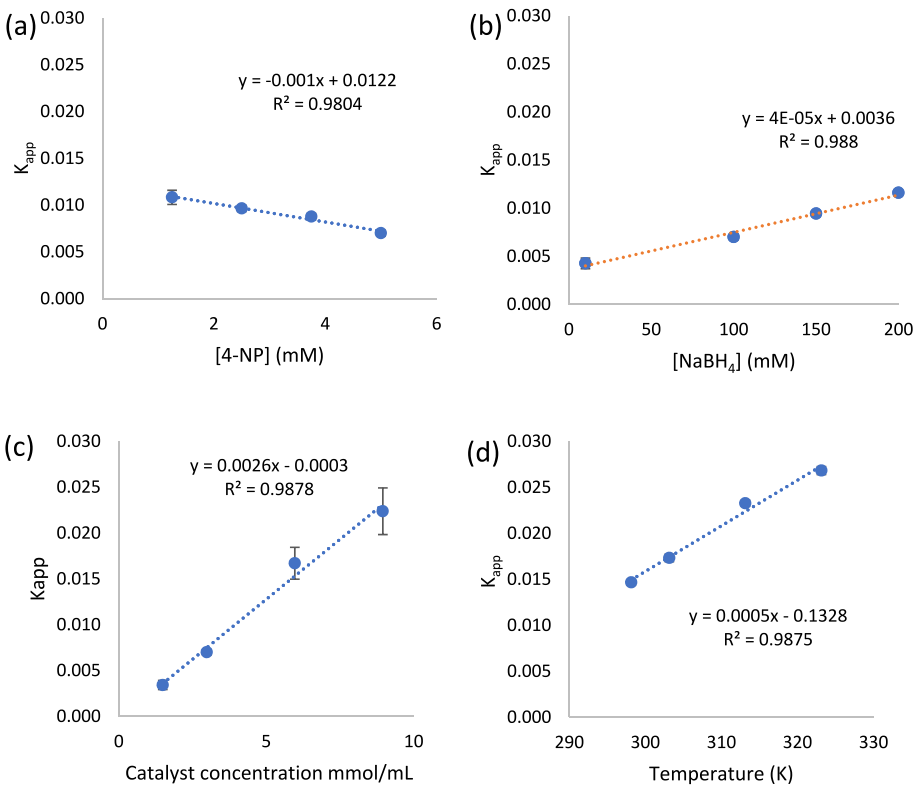

Fig. 6. Optimization of 4-NP reduction using **AL13** as a model catalyst. The reaction conditions investigated are (a) 4-NP concentration, (b) $NaBH_4$ concentration (c) catalyst concentration and (d)temperature.

Table 3
Thermodynamic parameters calculated for **AL13**.

Code	Ea_{app} (kJ/mol)	A	$\Delta H^{\ddagger}$ (kJ/mol)	$\Delta S^{\ddagger}$ (kJ/mol)	$\Delta G^{\ddagger}$ (kJ/mol @298.15 K)
AL13	19.6	41.1	17.0	−0.223	83.5

$$\ln(k_{app}) = \ln(\mathrm{A}) - \frac{Ea_{app}}{RT} \quad \text{Equation 2}$$

Eyring equation:

$$\ln\left(\frac{k_{app}}{T}\right) = -\frac{\Delta H^{\ddagger}}{R} \bullet \frac{1}{T} + \frac{\Delta S^{\ddagger}}{R} + \ln\frac{k_B}{h} \quad \text{Equation 3}$$

Gibbs equation:

$$\Delta G^{\ddagger} = \Delta H^{\ddagger} - \mathrm{T} \times \Delta S^{\ddagger} \quad \text{Equation 4}$$

The Arrhenius plot (Fig. 7) was used to determine the Ea_{app} and A. The Arrhenius equation (equation 2) shows that the slope of the Arrhenius plot is equivalent to $-\frac{Ea_{app}}{R}$. The apparent activation energy was thus determined as 19.6 kJ/mol. The Arrhenius equation further showed that the intercept is equal to $\ln(\mathrm{A})$. A was thus determined as 41.05.

The linear Eyring plot (Fig. 7) was used to determine $\Delta H^{\ddagger}$ and $\Delta S^{\ddagger}$ values. Equation (3) indicates that the slope of the Eyring plot is equal to $-\frac{\Delta H^{\ddagger}}{R}$, thus $\Delta H^{\ddagger}$ was determined as 17.0 kJ/mol. As the $\Delta H^{\ddagger}$ is positive this indicates that the reduction reaction is endothermic. The intercept of the Eyring plot is $= \frac{\Delta S^{\ddagger}}{R} + \ln\frac{k_B}{h}$ and as k_B, R and h are all constant $\Delta S^{\ddagger}$ was determined as −0.223 kJ/mol. This negative value indicates that more ordered structures are achieved during the rate determining step as the reagents are absorbed onto the NP surface. Lastly, the Gibbs equation (equation (4)) was used to determine the Gibbs free energy at 298.15 K as 83.5 kJ/mol. This is the energy required to move 4-NP to the activated state.

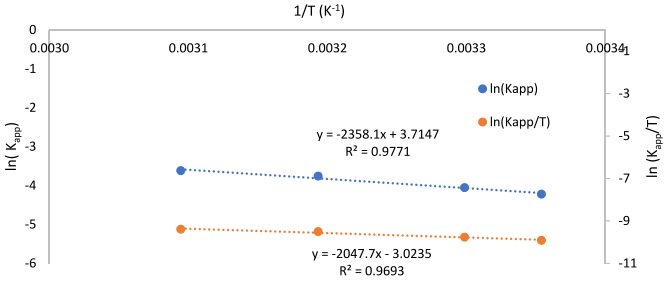

Fig. 7. Arrhenius and Eyring plot of **AL13** as converted form the temperate dependence studies.

3.3.2.2. Comparison of catalysts in 4-NP reduction. After investigating the reaction parameters in section 3.3.2.1., each of the 18 catalysts was evaluated under the optimized conditions. 100 μL of (5 mM) 4-NP was added to 1 mL of $NaBH_4$ (0.1 M) and the reaction made up to 4 mL with distilled water. The mixture was then subjected to the UV–Vis heating chamber to reach 298.15 K whereafter 10 μL of (5.97 mmol/L Ni/Cu) catalyst was introduced. The mixture was stirred, and the change in absorbance monitored at 400 nm. These reactions were all completed in quadruplicate to determine the average k_{app} and the respective R^2 values from its slope and the results shown in Fig. 8.

In this comparison study the Cu and Cu/Ni NPs both reduced the 4-NP without an induction time being present. The Ni coated SPIONs all showed the presence of an induction time. This time is defined as a period in which the NP restructures its surface to enable reduction to occur. This induction time, however varied depending on numerous factors. From the comparison studies shown in Fig. 8, a general increase in the k_{app} value is seen from Ni < Cu/Ni < Cu. This indicates that the Cu

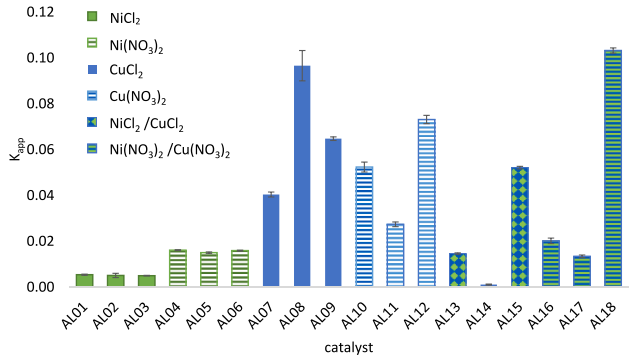

Fig. 8. k_{app} achieved for each $NiCl_2$ (solid green), $Ni(NO_3)_2$ (striped, green), $CuCl_2$ (solid blue), $Cu(NO_3)_2$ (striped, blue), $NiCl_2$/$CuCl_2$ (green/blue squares) and $Ni(NO_3)_2$/$Cu(NO_3)_2$ (green/blue stripes) catalyst. These comparison studies were done under optimized reaction conditions: 100 μL of 4-NP(5 mM), 1 mL of $NaBH_4$ (0.1 M), 10 μL of catalyst (5.97 mmol/L Ni/Cu) made up to 4 mL with distilled water and done at 298.15 K. (For interpretation of the references to color in this figure legend, the reader is referred to the Web version of this article.)

species are the active site on the Cu/Ni surface and a decrease in the Cu species due to substitution by Ni atoms resulted in a decrease in the k_{app} achieved.

Secondly, the use of different metal-to-SPION ratios was evaluated. For the Ni NPs (**AL02** vs. **AL03** and **AL05** vs. **AL06**) this had no significant effect on the k_{app} values but did however result in a decrease in the t_0. For the Cu and the Cu/Ni NPs this resulted in a drastic difference. This is due to only the surface atoms actively participating in the coordination and bonding of H_2 and 4-NP compounds, thus a thin shell (smaller metal-to-SPION ratio) has a higher percentage of surface atoms vs. inner shell atoms that are available for coordination to occur. As this study used a constant mol of Ni and Cu loading throughout it resulted in that more NPs were used in this reaction thus more surface atoms were present overall to facilitate the reaction.

Thirdly, we compared the use of different precipitating agents used in the synthesis of these catalysts. As seen from the FT-IR analysis, the hydrazine acts as a surface ion to stabilize the NP while the $NaBH_4$ only has the hydroxy counterions. These hydrazine NPs are generally smaller and together with lower metal loading resulted in higher K_{app} values for the Cu and Cu/Ni NPs.

Furthermore, the nitrate and chloride metal precursor salts were compared. These results showed increased k_{app} values for nitrates compared to chlorides. This can be due to multiple factors. Firstly, a generally smaller NP was achieved by the nitrate metal precursor compared to the chloride, as seen by the TEM analysis. Secondly, the ICP-OES showed generally lower Ni and Cu loadings achieved by the nitrates. Although these factors may contribute to the increased k_{app} value the main factor is the anion itself. This is evident from the Ni coated SPIONs as the change in size and Ni content per NP does not significantly change the k_{app} value, but a clear change is seen when considering the surface anions. Mikami et al. explained that the use of chlorides as NP precursor salt drastically decreased the catalyst reduction capability due to the Cl^- strongly coordinating to the NP thus prohibiting coordination from occurring. Polar anions such as SO_4^-, with the coordinating S atom being slightly positive, were however able to easily dissociate during catalysis allowing for more active sites to be available for H_2 and 4-NP to coordinate [28]. As NO_3^- coordinates in a similar manner with the N being partly positively charged it will dissociate from the positive metal ions on the NP surface much easier thus allowing for more coordination sites for reduction to occur.

AL08 proved to be an outlier in all of these trends as it showed a much higher k_{app} value than expected. This can be partially explained by the ICP-OES results that showed unexpected lower Cu content compared to the hydrazine analogue while simultaneously achieving higher Fe content. This resulted in more NPs being added to the reaction to achieve the same Cu content. Furthermore, it was observed that although the majority of the NPs are amorphous (Fig. 3 and Fig. S3) **AL08** does contain a lot of square NPs as seen in Fig. 9. The shape of a NP has been reported to influence its activity [29]. This should however be investigated further to determine whether this is indeed responsible for its unexpected high yield.

Overall, the bimetallic coated SPIONs (**AL18**) showed the best reduction capability as it achieved a k_{app} value of 0.103 s^{-1}. This value is very good when compared to other NPs used in 4-NP reduction (Table 4). The SPION@Ni/Cu catalyst is three times faster than monometallic Cu_{55} NPs reported by Matinise et al. [8] Utilizing Fe and Ni in the structure of the NP not only allows for easy recyclability but also drastically decreases the production cost of these NPs making these NPs much more attractive for industrial use. The catalyst was also compared to magnetic $CuFe_2O_4$ which incorporated the Cu as Fe–Cu alloy. This catalyst showed a slightly higher k_{app} value but used high catalyst loading, of almost 3 times higher, to achieve this slight increase [25]. This is due to the active Cu ions being incorporated into the core of the NP, thus much higher loadings are required to supply enough active sites for reduction to occur. Utilizing the Cu and Ni as a thin shell on the SPION surface thus allows for more of the active metals to be present on the NP surface. This core-shell structure is thus preferred as it can achieve similar activities at much lower catalyst loadings. Other heterogeneous supports for Ni and Cu NPs include sponges which achieved much lower k_{app} values [21].

*3.3.2.3. Recycling of **AL18**.* As **AL18** showed the fastest conversion of 4-NP to 4-AMP, we evaluated it in consecutive reactions to ensure that the catalyst is recyclable. As the optimized catalyst loading was too low to sufficiently isolate, wash and reuse in consecutive runs, new reaction parameters were identified to assess the recyclability. These parameters were 100 μL (2 mg/mL) catalyst, 100 μL (5 mM) 4-NP and 1 mL of $NaBH_4$ (0.05 M). During the first run it was seen that these new parameters introduced an induction time of 250 s whereafter rapid reduction took place within 70 s (Fig. 10). During the subsequent runs, this induction time was absent, however a small acceleration was still visible in the 250–320 s range. This is due to the NPs already being in its activated form after the first run. The recycling experiments show a 25 % decrease in the k_{app} value between run 1 to run 4 whereafter no significant decrease in k_{app} was observed.

4. Conclusion

In conclusion, this paper reports a fast, easy and cost-effective manner of producing SPION@Ni, SPION@Cu and SPION@Ni/Cu catalysts by simple impregnation methods. These immobilized nanocatalysts prove to be stable, without the use of expensive ligands, as no agglomeration was visible and proved to be highly reproducible in terms of NP size with small deviations of less than 5 nm in size. These NPs were evaluated in the reduction of 4-NP to 4-AMP and showed a general trend in activity SPION@Ni < SPION@Cu < SPION@Ni/Cu. It was also evident that smaller SPION-to-M ratios obtained better k_{app} values for the same active metal loading and nitrates resulted in faster reduction than the chloride analogues. This resulted in **AL18** being the overall best catalyst for the reduction of 4-NP to 4-AMP as it achieved a k_{app} of 0.103 s^{-1}. This catalyst was easily separated via magnetic decantation and reused for up to 10 consecutive runs.

CRediT authorship contribution statement

Anname Lourens: Data curation, Formal analysis, Investigation, Methodology, Validation. **Anzel Falch:** Writing – review & editing. **Rehana Malgas-Enus:** Conceptualization, Supervision.

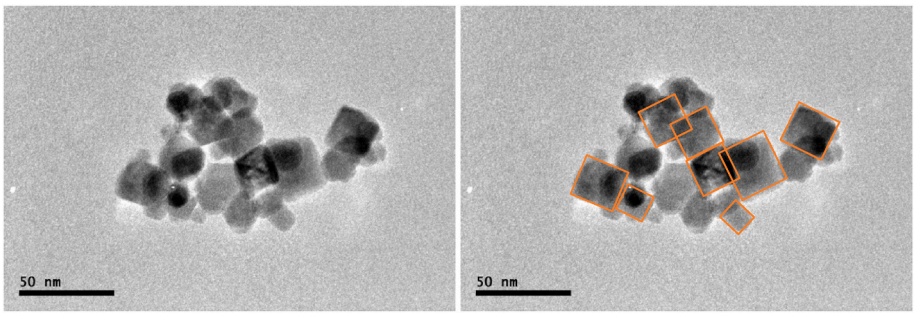

Fig. 9. HR-TEM of **AL08** indicating the square-like structure of the some of the NPs.

Table 4
Comparison of k_{app} values achieved in 4-NP reduction by SPIONs@Ni, SPIONs@Cu and SPIONs@Ni/Cu MNPs and other reported nano-catalysts.

NPs	Catalyst loading	k_{app} (s^{-1})	Recyclable	reference
SPIONs	0.0030 M	–		
AL03 SPIONs@Ni	0.015 M	0.005	Yes	Current work
AL06 SPIONs@Ni	0.015 M	0.016	Yes	Current work
AL09 SPIONs@Cu	0.015 M	0.065	Yes	Current work
AL12 SPIONs@Cu	0.015 M	0.073	Yes	Current work
AL15 SPIONs@Ni/Cu	0.015 M	0.052	Yes	Current work
AL18 SPIONs@Ni/Cu	0.015 M	0.103	Yes	Current work
Cu_{55}	0.0011 M	0.033	no	[8]
Cu-AG-sponge	20 mg	0.0054	Yes	[21]
Ni-AG-sponge	20 mg	0.0026	Yes	[21]
$CuFe_2O_4$	0.0425 M	0.12	Yes	[25]
C–Ni/500	5 mg	0.0186	Yes	[30]
C–Ni/350	0.4 mM	0.00178	Yes	[31]
Fe_3O_4–Ni/C	0.5 mg	0.00083	Yes	[31]
Ag@AHB	40 mg	0.0149	–	[32}
Ag@PEI@AHB	40 mg	0.0193	Yes	[32]
Cu@SiO_2@C–Ni/700,	0.2 mg	0.00931	yes	[33]

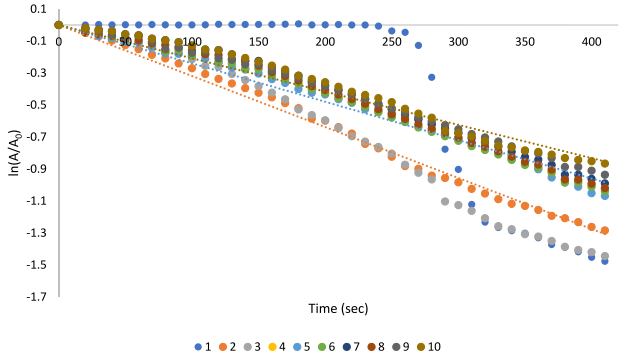

Fig. 10. Recyclability of **AL18** as seen by the $\ln(A/A_0)$ vs. time plots of the ten consecutive runs.

Declaration of competing interest

The authors declare the following financial interests/personal relationships which may be considered as potential competing interests: There are no conflicts to declare.

Rehana Malgas-Enus reports financial support was provided by University of the Witwatersrand Johannesburg.

Data availability

Data will be made available on request.

Acknowledgements

This work is based on the research supported in part by the *National Research Foundation* of South Africa (SRUG200224506537) as well as by the postgraduate funding department of Stellenbosch University (*SUPG*). Additionally, the authors express their gratitude to Dr. Adam Shnier for his contribution in conducting the XRD analysis and providing insightful interpretations.

Appendix B. Supplementary data

Supplementary data to this article can be found online at https://doi.org/10.1016/j.matchemphys.2024.129022.

References

[1] P. Xu, G.M. Zeng, D.L. Huang, C.L. Feng, S. Hu, M.H. Zhao, C. Lai, Z. Wei, C. Huang, G.X. Xie, Z.F. Liu, Use of iron oxide nanomaterials in wastewater treatment: a review, Sci. Total Environ. 424 (2012) 1–10.
[2] A. Lourens, A. filch, R. Malgas-Enus, Magnetite immobilized metal nanoparticles in the treatment and removal of pollutants from wastewater: a review, J. Mater. Sci. 58 (2023) 1–20.
[3] T.K. Das, N.C. Das, Advances on the catalytic reduction of 4-nitrophenol by nanostructured materials as benchmark reaction, Int. Nano Lett. 12 (2022) 223–242.
[4] M. Teimouri, F. Khosravi-Nejad, F. Attar, A.A. Saboury, I. Kostova, G. Benelli, M. Falahati, Gold nanoparticles fabrication by plant extracts: synthesis, characterization, degradation of 4-nitrophenol from industrial wastewater, and insecticidal activity–a review, J. Clean. Prod. 184 (2018) 740–753.
[5] S. Ganguly, P. Das, M. Bose, T.K. Das, S. Mondal, A.K. Das, N.C. Das, Sonochemical green reduction to prepare Ag nanoparticles decorated graphene sheets for catalytic performance and antibacterial application, Ultrason. Sonochem. 39 (2017) 577–588.
[6] V.S. Zaitsev, D.S. Filimonov, I.A. Presnyakov, R.J. Gambino, B. Chu, Physical and chemical properties of magnetite and magnetite-polymer nanoparticles and their colloidal dispersions, J. Colloid Interface Sci. 212 (1999) 49–57.
[7] A. Parashar, S. Sikarwar, R. Jain, Removal of pharmaceuticals from wastewater using magnetic iron oxide nanoparticles (IOPs), Int. J. Environ. Anal. Chem. 102 (2020) 117–133.
[8] N. Matinise, J.T. Khutlane, R. Malgas-Enus, The effect of magic number phosphine stabilized mono- and bimetallic Au, Cu and Au-Cu nanoparticles as catalysts in the reduction of 4-nitrophenol–A kinetic study, Nano-struct. Nano-Object. 29 (2022) 100814.
[9] E.A. Glazkova, O.V. Bakina, M.I. Lerner, A.V. Pervikov, Synthesis and applications of bimetallic nanoparticles of immiscible elements, Recent Pat. Nanotechnol. 12 (2018) 132–142.
[10] T. Mazhar, V. Shrivastava, R.S. Tomar, Green synthesis of bimetallic nanoparticles and its applications: a review, J. Pharm. Res. 9 (2017) 102–110.
[11] E.J. Lukhele, J.T. Khutlane, N.B. Bathori, R. Malgas-Enus, Reduction and removal of methylene blue from aqueous solutions via recyclable magnetic gold nanomaterials, Surface. Interfac. 31 (2022) 101970.
[12] K.J. Datta, A.K. Rathi, P. Kumar, J. Kaslik, I. Madrik, V. Ranc, R.S. Varma, R. Zboril, M.B. Gawande, Synthesis of flower-like magnetite nanoassembly: application in the efficient reduction of nitroarenes, Sci. Rep. 7 (2017) 1–17.

[13] J. Qiao, T. Wang, K. Zheng, E. Zhou, C. Shen, A. Jia, Q. Zhang, Magnetically reusable Fe_3O_4@NC@Pt catalyst for selective reduction of nitroarenes, Catalysts 11 (2021) 1219.
[14] V. Hajdu, A. Prekob, G. Muranszky, I. Kocserha, Z. Konya, B. Fiser, B. Viskolcz, L. Vanyorek, Catalytic activity of maghemite supported palladium catalyst in nitrobenzene hydrogenation, React. Kinet. Mech. Catal. 129 (2020) 107–116.
[15] D. Xu, M. Xiong, M. Kazemnejadi, Efficient reduction of nitro compounds and domino preparation of 1-substituted-1H-1,2,3,4-tetrazoles by Pd(II)-polysalophen coated magnetite NPs as a robust versatile nanocomposite, RSC Adv. 11 (2021) 12484–12499.
[16] M.N. Shikh, A. Helal, A. Helal, A.N. Kalanthoden, B. Najjar, M.A. Aziz, H. D. Mohamed, Sub-nanometric Rh decorated magnetic nanoparticles as reusable catalysts for nitroarene reduction in water, Cat, COM 119 (2019) 134–138.
[17] H.-F. Chen, M.-L. Hung, T.-H. Hung, Y.-W. Tsai, C.-W. Su, J. Yang, G.G. Huang, single-step preparation of silver-doped magnetic hybrid nanoparticles for the catalytic reduction of nitroarenes, ACS Omega 3 (2018) 3340–3347.
[18] R. Antony, R. Marimuthu, R. Murugavel, Bimetallic nanoparticles anchored on core-shell support as an easily recoverable and reusable catalytic system for efficient nitroarene reduction, ACS Omega 4 (2019) 9241–9250.
[19] B. Zeynizadeh, I. Mahammadzadeh, Z. Shokri, S. Ali Hosseini, Synthesis and characterization of $NiFe_2O_4$@Cu nanoparticles as a magnetically recoverable catalyst for reduction of nitroarenes to arylamines with $NaBH_4$, J. Colloid Interface Sci. 500 (2017) 285–293.
[20] A. Lourens, D. Otto, A. Falch, R. Malgas-Enus, Magnetic styrene polymers as recyclable oil absorbents, obtained via living polymerization of styrene on the surface of Ni and Cu nanoparticles inorg, Chem. Commun. 142 (2022) 109586.
[21] T. Kamal, A.M. Asiri, N. Ali, Catalytic reduction of 4-nitrophenol and methylene blue pollutants in water by copper and nickel nanoparticles decorated polymer sponges, Spectrochim. Acta Mol. Biomol. Spectrosc. 261 (2021) 120019.
[22] A.I. Ayad, D. Luart, A.O. Dris, E. Guenin, Kinetic analysis of 4-nitrophenol reduction by "water-soluble" palladium nanoparticles, Nanomaterials Basel 10 (2020) 1169.
[23] A. Rostami-Vartooni, A. Moradi-Saadatmand, M. Mahdavi, Catalytic reduction of organic pollutants using biosynthesized Ag/C/Fe_3O_4 nanocomposite by red water and *Caesalpinia gilliesii* flower extract, Mater. Chem. Phys. 219 (2018) 329–339.
[24] M. Kohantorabi, M.R. Gholami, Kinetic analysis of the reduction of 4-nitrophenol catalyzed by CeO_2 nanorods-supported CuNi nanoparticles, Ind. Eng. Chem. Res. 56 (2017) 1159–1167.
[25] J. Feng, L. Su, Y. Ma, C. Ren, Q. Guo, X. Chen, $CuFe_2O_4$ magnetic nanoparticles: a simple and efficient catalyst for the reduction of nitrophenol, Chem. Eng. J. 221 (2013) 16–24.
[26] S. Wunder, F. Polzer, Y. Lu, Y. Mei, M. Ballauff, Kinetic analysis of catalytic reduction of 4-nitrophenol by metallic nanoparticles immobilized in spherical polyelectrolyte brushes, J. Phys. Chem. C 114 (2010) 8814–8820.
[27] N. Bingwa, R. Meijboom, Evaluation of catalytic activity of Ag and Au dendrimer-encapsulated nanoparticles in the reduction of 4-nitrophenol, J. Molecular Cat. A: Chem 369 (2015) 1–7.
[28] T. Ishii Mikami, F. Kitamura, A. Masunga, Effect of other anions on reduction of nitrate in water over Pd–In catalyst loaded on various supports, IOP Conf. Ser. Earth Environ. Sci. 427 (2020) 012004.
[29] S. Mostafa, F. Behafarid, J.R. Croy, L.K. Ono, L. Li, J.C. Yang, A.I. Frenkel, B. Roldan Cuenya, Shape-dependent catalytic properties of Pt nanoparticles, J. Am. Chem. Soc. 132 (2010) 15714–15719.
[30] M. Zhang, L. Ding, J. Zheng, L. Liu, H. Alsulami, M.A. Kuthbi, J. Xu, Surface modification of carbon fibers with hydrophilic Fe_3O_4 nanoparticles for nickel-based multifunctional composites, Appl. Surf. Sci. 509 (2020) 1453448.
[31] L. Ding, L. Yang, J. Xu, J. Zheng, M. Zhang, Controllable compositions and structures of Fe_xO_y@SiO_2@C-Ni hybrids with a silica layer as a mineral redox buffer, Inorg. Chem. 60 (2021) 8880–8889.
[32] C. Gao, Q. An, Z. Xiao, S. Zhai, B. Zhai, Z. Shi, Alginate and polyethyleneimine dually mediated synthesis of nanosilver-containing composites for efficient p-nitrophenol reduction, Carbohydr. Polym. 181 (2018) 744–751.
[33] L. Ding, J. Hub, Y. Zhanga, J. Xub, M. Zhang, Copper-based nanocatalysts with SiO_2 and carbon dual-layer coatings and metallic Ni/CuNi decoration toward highly efficient nitroaromatics reduction, Inorg. Chem. 61 (3) (2022) 1717–1727.